Nanoporous Carbide Derived Carbon with Tunable Pore Size

Y. Gogotsi[1*], A. Nikitin[1], H. Ye[1], W. Zhou[2], J. E. Fischer[2], B. Yi[3], H. C. Foley[3], M. W. Barsoum[1]

During the past decades major efforts in the field of porous materials have been directed toward control of the size, shape and uniformity of the pores. Carbide-derived carbons (CDCs) represent a new class of nanoporous carbons with porosity that can be tuned with sub-Ångström accuracy in the range 0.5-2 nm. CDCs have a more narrow pore size distribution than single-wall carbon nanotubes or activated carbons; their pore size distribution is comparable with that of zeolites. CDCs are produced at temperatures from 200-1200ºC as a powder, a coating, a membrane or parts with near-final shapes, with or without mesopores. They can find applications in molecular sieves, gas storage, catalysts, adsorbents, battery electrodes, supercapacitors, water/air filters and medical devices.

Porous solids are of great technological importance due to their ability to interact with gases and liquids not only at the surface, but throughout their bulk[1]. While large pores can be produced and well controlled in a variety of materials[2], nanopores in the

[1] Department of Materials Engineering, Drexel University, Philadelphia, Pennsylvania 19104, USA
[2]Department of Materials Science and Engineering, University of Pennsylvania, Philadelphia, Pennsylvania 19104, USA
[3]Department of Chemical Engineering, The Pennsylvania State University, University Park, Pennsylvania 16801, USA
*Correspondence should be addressed to Y.G (e-mail: gogotsi@drexel.edu)

range of 2 nm and below (micropores, according to IUPAC classification) are usually achieved only in carbons or zeolites. Highly crystallized zeolites have a narrow pore size distribution, but discrete pore sizes and the fine-tuning of pore size are impossible in zeolites because pores are controlled by a lattice structure. Activated carbons may have pore diameters down to 0.5 nm[3], or mesopores of several nanometers, but they typically have a broad pore size distribution[4] that limits their ability to separate molecules of different sizes. Pore sizes of 0.3-0.7 nm have been demonstrated in carbon membranes, but with little control over the distribution of pore sizes[5].

To the best of our knowledge, materials with a tunable pore structure at the atomic level and a narrow pore size distribution do not exist. Such solids would be invaluable for gas storage, batteries, supercapacitors and many nanotechnological applications. Porous carbons are usually made by thermal decomposition of organic materials. More recently, it has been shown that selective etching of carbides is an attractive technique for the synthesis of various carbon structures from nanotubes[6] to diamonds[7]. Carbon produced by the extraction of metals from carbides is called carbide-derived carbon (CDC). Leaching in supercritical water[8] or high-temperature treatment in halogens[9] has been used to remove metals from carbides producing carbon coatings, powders or components. The linear reaction kinetics of the chlorination of carbides[10] allows transformations to large depth, until the particle or component is completely converted to carbon. Since the rigid metal carbide lattice is used as a template and the metal is extracted layer-by-layer, atomic level control can be achieved in the synthesis process and the carbon structure can be templated by the carbide structure. Further structure modification and control can be achieved by varying the temperature, gas composition,

and other process variables. An important advantage of the CDC process is that the transformation is conformal and does not lead to changes in sample size or shape. Unlike carbons of organic origin, CDCs produced by chlorination do not contain hydrogen.

The reaction

$$SiC + 2Cl_2 = SiCl_4 + C \quad (1)$$

has been used for the production of silicon tetrachloride since 1918[11]. The remaining carbon was usually burned. During the last decades, various CDCs have been investigated by several groups and specific surface areas (SSA) of up to 2000 m^2/g with small pore sizes have been reported[9,12-14]. Comparison of scattered literature data on CDCs shows that, for different carbides (SiC, TiC, ZrC, B_4C, TaC, Mo_2C and many others) and chlorination temperatures, pores of any size between 0.8 and 2.1 nm, determined by the structure of the carbide precursor and process parameters, were produced. However, those were scattered points. No control over the pore structure has been reported. The **objective** of this work is to demonstrate precise pore size tuning in CDCs by controlling the synthesis temperature.

Although many carbides can be used to produce CDCs, this study was conducted on Ti_3SiC_2 powders and bulk samples. Ti_3SiC_2 is a soft ceramic with a lamellar structure (Supplement 1) that is commercially available and can easily be machined to any shape[15]. Etching of Ti_3SiC_2 can generate a larger pore volume (~75%) compared to TiC or SiC (56.2% and 57.3%, respectively), as shown in Supplement 2. Interaction of this carbide with chlorine, Cl_2, has not been reported in the literature.

Chlorination in a flow of pure Cl_2 for 3 hours in a quartz tube furnace results in extraction of Ti and Si from Ti_3SiC_2 leading to the formation of carbon by the reaction

$$Ti_3SiC_2 + 8Cl_2 = SiCl_4 + 3TiCl_4 + 2C \quad (2)$$

Four different techniques were independently used to measure the pore size: Ar, N_2 and methyl chloride, CH_3Cl, sorption, as well as small-angle X-ray scattering (SAXS), as described in Methods. As can be seen in Fig. 1, pore sizes of CDCs increase with increasing temperature, from 0.51 nm at 300ºC, to 0.64 nm at 700ºC and 1.10 nm at 1100ºC. The sorption isotherms of low-temperature CDCs (up to 600°C) obtained using N_2, Ar, or, CH_3Cl, were of type I in the Brunauer classification, which is evidence of the presence of nanopores and the absence of meso- or macropores. This is in agreement with the differential pore size distributions shown in Fig. 1a. Very small pore sizes were achieved at low temperatures; just slightly larger than the interplanar spacing in graphite (0.3354 nm). It is close to the smallest nanotubes reported and is smaller than the inner cavity of C_{60} fullerenes. What is even more impressive is the fact that the pore size distributions are very narrow. The distributions shown in Fig. 1a are equivalent to, or more narrow than, those of VPI-5 zeolite[1].

Isotherms of CDCs produced above 700°C were of type IV, which indicates the presence of mesopores. Total pore volumes observed for the samples produced at 700°, 900°, and 1100°C were almost the same, but the pore size distributions were different: Mesopore volume and size increased with increasing chlorination temperatures. Their equivalent radius was less than 3 nm at 700ºC (Fig. 1a) and about 6 nm at 1100ºC (Fig. 1b). Weight loss and energy-dispersive X-ray spectroscopy analysis of the samples after chlorination suggested almost complete removal of Ti and Si above 400ºC. Since the CDCs retained the original volume of the carbide precursor, it is fair to assume the total pore volume to be the same after chlorination at different temperatures. The maximum

pore volume of ~0.64 cm^3/g accessible to Ar and N_2 in CDC after heat-treatment at 700-1200°C is in agreement with the theoretically calculated value of 0.645 cm^3/g.

SAXS measurements confirm the evolution of pore size with increasing processing temperature and also suggest a change in pore shape at the highest temperatures. In Fig. 2, we plot the data for 7 samples spanning the range between 300°C and 1200°C. The results have been corrected for background and scattering by the quartz container. We observe almost monodisperse Guinier behavior, $\log(I) \sim - Q^2(R_g)^2/3$ over a broad range of Q^2 (Fig. 2a), as evidenced by the fact that the analysis after[16] gives a very narrow peak in $m(R_g)$ which accounts for most of the nanopore volume (Fig. 2b). SAXS confirms the aforementioned sorption data and shows that *pore size can be controlled with better than 0.05 nm accuracy* (Fig. 2c) – a remarkable result that has never been demonstrated for any other porous material.

The interpretation of R_g (Fig. 2c) depends on the shape of the nanopores. For spheres with diameter 2R, $R_g = 0.77R$, while for slit pores approximated as cylinders of radius R and height D, $R_g^2 = D^2/12 + R^2/2$. The analysis of the CH_3Cl sorption data assumed slit pores, which implies that the sizes in Fig. 1 are associated with the height of the slits. Slit pores are the logical choice for temperatures up to 800ºC, given the layered nature of the precursor material (Supplement 1) and the persistence of weak interlayer correlations for low temperatures shown by XRD (Supplement 3). A kinetic model of self-organization in the formation of nanopores during chlorination of SiC was proposed in ref. 13. It can be used to describe the formation of the ordered nanoporous carbon from Ti_3SiC_2. With increasing temperature, the specific distance for jump of carbon atoms increases and the pore size increases accordingly. More equiaxial pores form in the

1000-1200ºC temperature range (Fig. 2c), which is consistent with XRD data (supplement 3) that show complete loss of interlayer correlations such that the pores no longer retain any memory of the precursor lattice.

Microstructural studies of CDCs were conducted to explain their structural reorganization and the development of their porous structure with temperature. Raman spectroscopy (Fig. 3a,b) shows that carbon already forms at 200ºC. However, XRD (Supplement 3) shows peaks of the initial carbide; thus the transformation was not complete at this temperature. A low position of G-band and upshifed D-band in the Raman spectrum (Fig. 3a) may be the result of carbon bonding to Si and significant sp^3 hybridization of carbon[17]. Si (<15%) was detected by EDS in the samples chlorinated at 300ºC, showing that Ti was preferentially etched at lower temperatures. Different rates of Si and Ti reaction were also observed in carburization and silicidation of Ti_3SiC_2 above 1400ºC[18]. Experiments on TiC[19] and SiC[20] show that Ti can be extracted by Cl_2 at lower temperatures than Si. Temperatures above 400ºC and 600ºC, respectively, were required for the conversion of nanocrystalline and microcrystalline SiC to CDC. Complete removal of Si from CDC and a decreased amount of trapped chlorine leads to an increase in pore volume from 0.25 cm^3/g at 300ºC to 0.645 cm^3/g at 700ºC. A slow increase in intensity and downshift of the D-band in the Raman spectra are observed with increasing temperature. According to high-resolution TEM analysis and selected area diffraction, the CDC samples produced at lower temperatures were completely amorphous (Fig. 3e). Noticeable ordering of graphite starts at 700ºC (Fig. 3d) and nanocrystalline graphite appears at 1200ºC (Fig. 3c). Thus, the L_a values can be calculated using the Tuinstra and Koenig equation from Fig. 3b only above 700ºC,

because this equation is not valid for amorphous carbon[17]. The FWHM of the G-band decreases slightly above 600ºC, but only at 1200ºC does Raman spectroscopy show the formation of ordered graphitic carbon. Very thin (2-5 graphene layers) sheets of graphite are clearly seen in TEM (Fig. 3c). The degree of graphitization depends on the duration of the chlorination process and slightly increases with time, but only at temperatures well above 1000ºC because of a very low mobility of carbon atoms below 1000ºC.

Total volume and characteristic dimensions of meso- and nanopores can be predicted and achieved by selection of a binary or ternary carbide or a carbide solid solution and variation of the chlorination process parameters. For example, carbon derived from SiC at 900ºC has a narrow size distribution and an average pore size of 0.65 nm, similar to CDCs produced from Ti_3SiC_2 at 700ºC, but with no mesopores. Carbon made from SiC at 1200ºC had a pore size of 1.2 nm, and values from 0.8 to 2.1 nm were reported in literature for SiC and B_4C derived carbons[21]. Depending on the carbide structure (Supplement 2), the pore volume of CDCs can vary from ~50% to ~80%. CDCs derived from Ti_3SiC_2 have the theoretical density of 0.55 g/cm^3 and porosity of 75.5%. CDC samples are hydrophilic and adsorb water quickly; rapidly sinking in water. However, if the surface is sealed with nail polish, they float because their density is well below 1 g/cm^3.

It is notable that CDCs do not have macroporosity if produced from a dense ceramic (Fig. 4) or a carbide single crystal. However, a controlled amount of macroporosity can be introduced by using sintered porous ceramics or pressed and pre-sintered compacts. Macroporosity or mesoporosity that appears at high chlorination

temperatures is not desirable for molecular sieve membranes, but would be necessary for catalytic and some other applications, because it allows easier access to nanopores.

Based on their tunable porous structures, controlled surface chemistry, and other properties, CDCs may be used for some applications where single-wall carbon nanotubes are currently considered[22]. For example, CDCs is an attractive material for electrodes for electrochemical double-layer capacitors commonly called "supercapacitors"[23]. Among the major advantages of CDCs are their high SSA, high conductivity, and controlled pore size distribution—which can be tuned to match various electrolytes. Strength and mechanical stability, two other necessary conditions of electrode performance, can be achieved in CDC as well.

Finally, it is known that hydrogen uptake depends on the porous structure of the adsorbent. The highest uptake was achieved in nanoporous carbons with SSA above 1000 m^2/g and almost no mesopores[24,25]. CDCs produced at 600ºC and 1100ºC have SSA of 1061 m^2/g and 1431 m^2/g, respectively. Our ability to tune the pore size to exactly fit the hydrogen (or other gas) molecule may be of principal importance for gas storage applications. About 40 wt.% Cl_2 is trapped in CDCs produced at 300-400ºC at room temperature and ambient pressure, if the cooling is done in argon, and it can reach 55-60 wt.% when cooled in Cl_2. The amount of Cl_2 stored decreases with increasing pore size, reaching less than 5 wt.% at 1200ºC (Supplement 4). The stored chlorine is slowly released, and its amount goes down to ~20 wt.% after storage for ten days in open air. Fast release of atomic chlorine is observed upon heating in Helium up to 600ºC at 10ºC/min. Attempts to measure SSA of CDC produced at 300ºC by the BET method resulted in the unreasonably low values of 162 m^2/g for N_2 and 382 m^2/g for Ar. This

clearly shows the selectivity of CDC to different gases. A significant volume of nanopores inaccessible to large molecules may allow for the separation of hydrogen from N_2 and other gases. It is also worth noting that the combination of near-net shape and very mild chlorination temperatures are not only unique to Ti_3SiC_2, but also bode well for the inexpensive mass production of CDC components, which, unlike zeolites, can have a large size and complex shape.

Methods

Total pore volume (V_Σ) and average pore size were calculated from Ar and CH_3Cl adsorption isotherms according to BJH (Barret, Joyner, and Halenda) theory. Specific surface area - according to BET (Brunauer, Emmet, and Teller) theory and nanopore volume – was calculated by using t-plots based on the CH_3Cl or Ar sorption isotherms. Nitrogen adsorption did not produce reliable results on samples with a pore size smaller than 1 nm. Ar adsorption (Micromeretics ASAP Pore Analyzer) was used to measure pore sizes above and under 1 nm using a spherical pore model, but the technique required long periods of time (5 days) for equilibration and could not produce the full distribution when the pore size approached 0.5 nm. The methyl chloride adsorption isotherms[26] were used to measure the pore size below 0.7 nm assuming a slit pore shape.

Small-angle X-ray scattering (SAXS) was performed on a multi-angle diffractometer equipped with a Cu rotating anode, double-focusing optics, evacuated flight path and 2-D wire detector. Data were collected over the Q range 0.005-1.4 $Å^{-1}$. Powder samples were loaded into 1.5-mm-diameter quartz capillary tubes and measured in transmission for 1 hour. The scattering intensity from an empty capillary was then collected and subtracted with sample absorption corrected. Expecting a finite but narrow distribution of radii of gyration R_g, we used a modified Guinier analysis to obtain the mean pore size and distribution[16]. The fraction volume of pores of a given size was then estimated for each sample. By deconvoluting the experimental ln(I) vs. Q^2 curves into

components corresponding to pores with different R_g, distribution functions of R_g were found.

Raman microspectroscopy (Renishaw 1000, Ar ion laser, 514.5 nm), transmission electron microscopy (TEM, JEOL 2010F), energy-dispersive spectroscopy (EDS) and X-ray diffraction (XRD, Siemens), were used to study the structure of CDC powders. In-plane crystal size of graphite L_a was calculated by the Tuinstra and Koenig equation[27]: $1/L_a=I_D/I_G$, where I_D and I_G are intensities of disorder-induced D band and graphite G band, assigned to zone center phonons of E_{2g} symmetry[17].

References and Notes

1. Davis, M. E. Ordered porous materials for emerging applications. *Nature* **417**, 813-821 (2002).
2. Joo, S. H. et al. Ordered nanoporous arrays of carbon supporting high dispersions of platinum nanoparticles. *Nature* **412**, 169-172 (2001).
3. Claye, A. & Fischer, J. E. Short-range order in disordered carbons: where does the Li go? *Electrochimica Acta* **45**, 107-120 (1999).
4. Rodriguez-Reinoso, F. & Sepulveda-Escribano, A. in *Handbook of Surfaces and Interfaces of Materials* (ed. Nalwa, H. S.) 309-355 (Academic Press, San Diego, 2001).
5. Shiflett, M. B. & C.Foley, H. Ultrasonic Deposition Of High-Selectivity Nanoporous Carbon Membranes. *Science* **285**, 1902-1905 (1999).
6. Derycke, V., Martel, R., Radosavljević, M., Ross, F. M. & Avouris, P. Catalyst-Free Growth of Ordered Single-Walled Carbon Nanotube Networks. *Nano Lett.* **2**, 1043-1046 (2002).
7. Gogotsi, Y., Welz, S., Ersoy, D. A. & McNallan, M. J. Conversion of Silicon Carbide to Crystalline Diamond-Structured Carbon at Ambient Pressure. *Nature* **411**, 283-287 (2001).
8. Gogotsi, Y. G. & Yoshimura, M. Formation of carbon films on carbides under hydrothermal conditions. *Nature* **367**, 628-630 (1994).
9. Gogotsi, Y. G., Jeon, J. D. & McNallan, M. J. Carbon coatings on silicon carbide by reaction with chlorine-containing gases. *J. Mater. Chem.* **7**, 1841-1848 (1997).
10. Ersoy, D., McNallan, M. J. & Gogotsi, Y. G. Carbon coatings produced by high temperature chlorination of silicon carbide ceramics. *, Mater. Res. Innovations* **5**, 55-62 (2001).
11. Hutchins, O. US Patent 1271713 (1918).

12. Boehm, H. P. & Warnecke, H. H. in *Proc. 12th Biennial Conf. on Carbon* 149-150 (Pergamon, Oxford, 1975).
13. Gordeev, S. K., Kukushkin, S. A., Osipov, A. V. & Pavlov, Y. V. Self-Organization in the Formation of a Nanoporous Carbon Material. *Phys. Solid State* **42**, 2314-2317 (2000).
14. Fedorov, N. F. Untraditional Solutions in Chemical Technology of Carbon Adsorbents. *Russ. Chem. J.* **39**, 73-83 (1995).
15. Barsoum, M. W. The $M_{n+1}AX_n$ Phases: A new class of solids. *Prog. Solid St. Chem* **28**, 201-281 (2000).
16. Kyutt, R. N., Smorgonskaya, E. A., Danishevski, A. M., Gordeev, S. K. & Grechinskaya, A. V. Structural Study of Nanoporous Carbon Produced from Polycrystalline Carbide Materials: Small-Angle X-Ray Scattering. *Phys. Solid State* **41**, 1359-1363 (1999).
17. Ferrari, A. C. & Robertson, J. Interpretation of Raman spectra of disordered and amorphous carbon. *Phys. Rev. B* **61**, 14095-14107 (2000).
18. El-Raghy, T. & Barsoum, M. W. Diffusion kinetics of the carburization and silicidation of Ti_3SiC_2. *J. Appl. Phys.* **83**, 112-119 (1998).
19. Leis, J., Perkson, A., Arulepp, M., Nigu, P. & Svensson, G. Catalytic Effect of Metals of the Iron Subgroup on the Chlorination of Titanium Carbide to Form Nanostructural Carbon. *Carbon* **40**, 1559-1564 (2002).
20. Gogotsi, Y. et al. Formation of Carbon Coatings on SiC Fibers by Selective Etching in Halogens and Supercritical Water. *Ceram. Eng. Sci. Proc.* **19**, 87-94 (1998).
21. Yanul', N. A. et al. Nanoporous Carbon Materials with Varied Porosity and Specific Features of Their Interaction with Water. *Russ. J. Appl. Chem.* **72**, 2159-2163 (1999).
22. Baughman, R. H., Zakhidov, A. A. & Heer, W. A. d. Carbon Nanotubes - the Route Toward Applications. *Science* **297**, 787-792 (2002).
23. Burke, A. Ultracapacitors: Why, How, and Where Is the Technology? *J. Power Sources* **91**, 37-50 (2000).
24. Nijkamp, M. G., Raaymakers, J. E. M. J., van Dillen, A. J. & de Jong, K. P. Hydrogen Storage Using Physisorbtion - Materials Demands. *Appl. Phys. A.* **72**, 619-623 (2001).
25. Schlapbach, L. & Züttel, A. Hydrogen-Storage Materials for Mobile Applications. *Nature* **414**, 353-358 (2001).
26. Mariwala, R. K. & Foley, H. C. Calculation of Micropore Sizes in Carbogenic Materails from the Methyl Chloride Adsorption Isotherm. *Ind. Eng. Chem. Res.* **33**, 2314-2321 (1994).
27. Tuinstra, F. & Koenig, J. L. Raman spectrum of graphite. *J. Chem. Physics* **53**, 1126-1130 (1970).

Acknowledgements

Thanks are due to Prof. W.-H. Shih, Drexel University, for help with nitrogen BET measurements. The work at Drexel University was supported by DARPA via ONR contract. The TEM used is operated by the Regional Materials Characterization Facility at the University of Pennsylvania. Purchase of the Raman spectrometer and SEM were supported by NSF grants DMR-0116645 and BES-0216343.

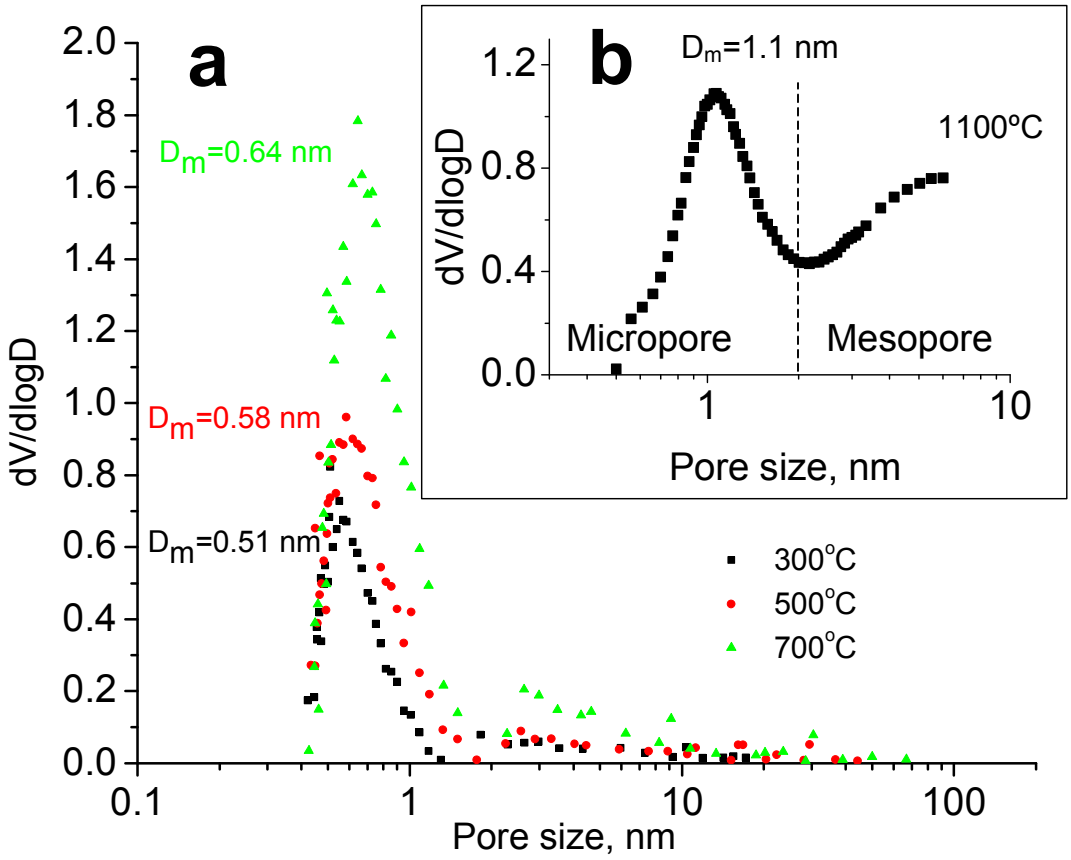

Fig. 1. Differential pore size distributions measured by **a**, methyl chloride and **b**, argon adsorption technique. No mesopores or macropores were detected at 300-500ºC. A small volume of mesopores of 2-4 nm in size appears at 700ºC, and the volume of mesopores increases sharply at 1100ºC and above. Distributions in Fig. 1a were calculated assuming a slit pore model. The pore size distribution in Fig. 1b was calculated according to the Horvath - Kawazoe method for spherical pore geometry. Ar adsorption was measured at -186ºC.

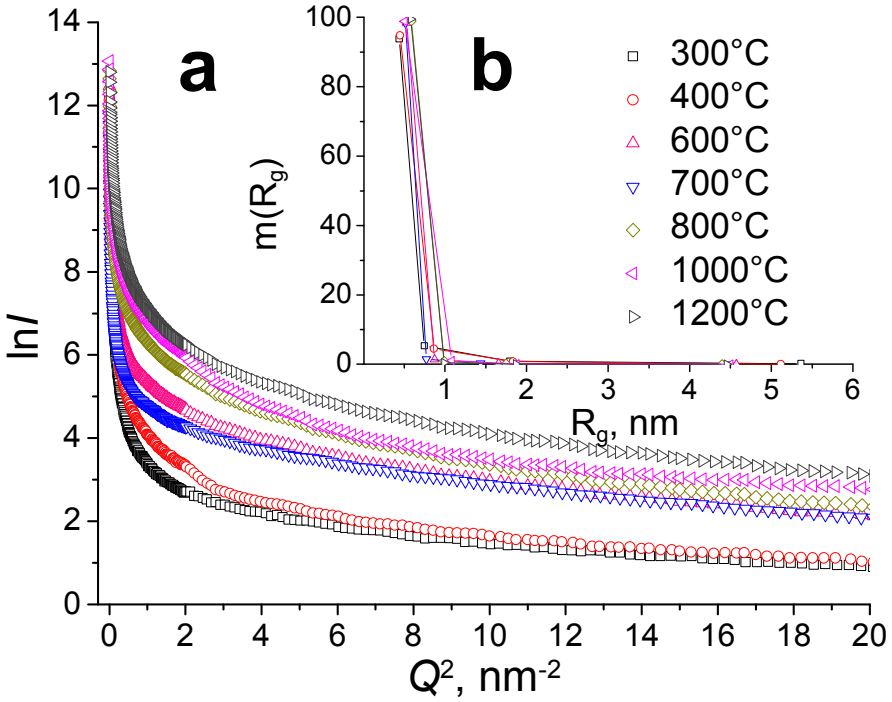
a
b
ln/
Q², nm⁻²
m(R_g)
R_g, nm
300°C
400°C
600°C
700°C
800°C
1000°C
1200°C

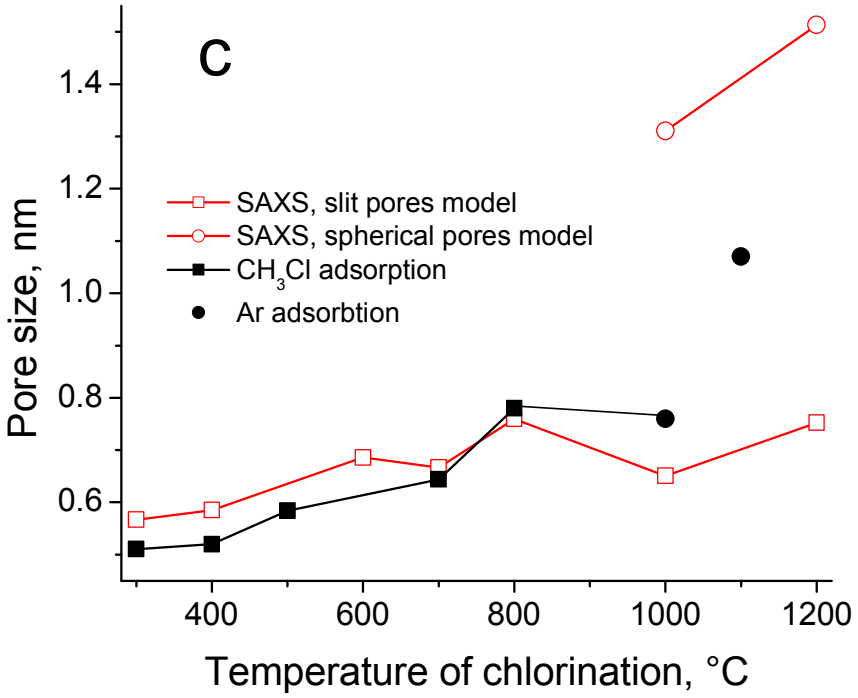
c
Pore size, nm
Temperature of chlorination, °C
SAXS, slit pores model
SAXS, spherical pores model
CH3Cl adsorption
Ar adsorbtion

Fig. 2. a, Experimental SAXS curves in Guinier coordinates, **b**, distribution of gyration radius m(R_g), and **c**, comparison of pore sizes obtained by CH_3Cl sorption and SAXS for different chlorination temperatures of Ti_3SiC_2. No pores with R_g larger than 0.6 nm were detected by SAXS. The SAXS-derived R_g at 600°C is 0.53 nm, while the sorption-based D_m (average of 500ºC and 700ºC values) is 0.61 nm. Taking the latter as the height of slit pores, the implied R is 0.71 nm, comparable to the radii of slit-shaped nanopores in polymer-derived materials[4]. Thus, slit pores have been formed between 300 and 1000°C. Conversely, at 1100°C we have R_g = 0.58 nm from SAXS, implying for *spherical* pores that 2R = D_m = 1.5 nm, ~30% greater than the measured value D_m = 1.1 nm but close to the median pore value of 1.56 nm for this temperature. We conclude that the pore shapes become more equiaxial at some temperature above 1000°C. Extremely fine tuning of pore sizes is possible between 300°C and 1000°C.

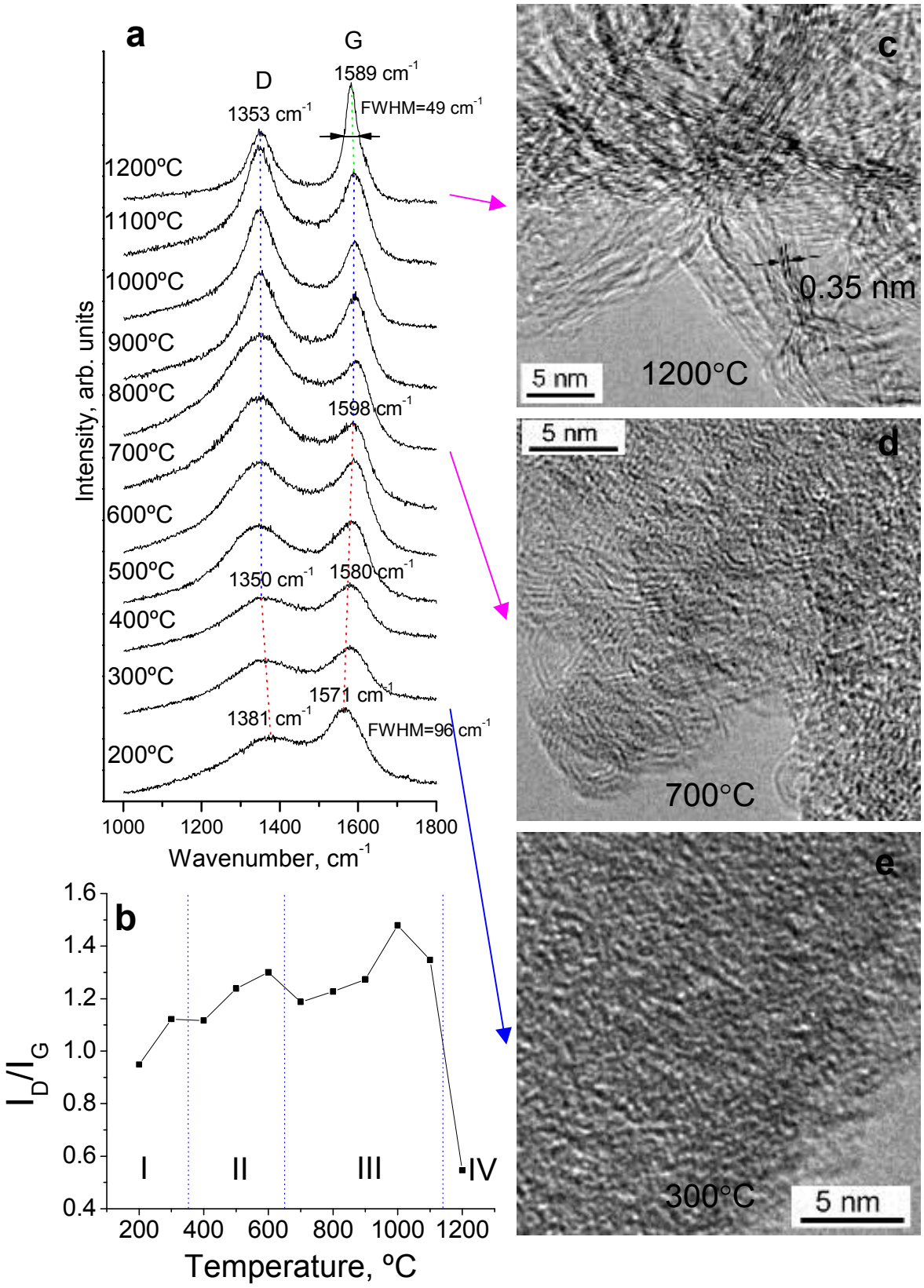
a
G
D
1589 cm-1
1353 cm-1
FWHM=49 cm-1
1200ºC
1100ºC
1000ºC
900ºC
800ºC
1598 cm-1
700ºC
600ºC
500ºC
1350 cm-1
1580 cm-1
400ºC
300ºC
1571 cm-1
1381 cm-1
FWHM=96 cm-1
200ºC
Intensity, arb. units
1000
1200
1400
1600
1800
Wavenumber, cm-1
b
1.6
1.4
1.2
1.0
0.8
0.6
0.4
ID/IG
I
II
III
IV
200
400
600
800
1000
1200
Temperature, ºC
c
0.35 nm
5 nm
1200°C
d
5 nm
700°C
e
300°C
5 nm

Fig. 3. a, Raman spectra of CDC synthesized at different temperatures, **b**, temperature dependence of I_D/I_G ratio and **c-e**, TEM images showing evolution of the carbon structure with temperature. **c,** 300ºC, **d**, 700ºC, **e**, 1200ºC. CDC produced in temperature range I (300ºC) is completely amorphous. Slow pore growth occurs in range II. Formation of carbon fringes at 700ºC and higher temperatures shows the beginning of the structure ordering leading to increasing pore size and appearance of mesopores in range III. Pronounced graphitization is observed at 1200ºC (range IV), resulting in a sharper G-band in the Raman spectrum and decreased I_d/I_g ratio.

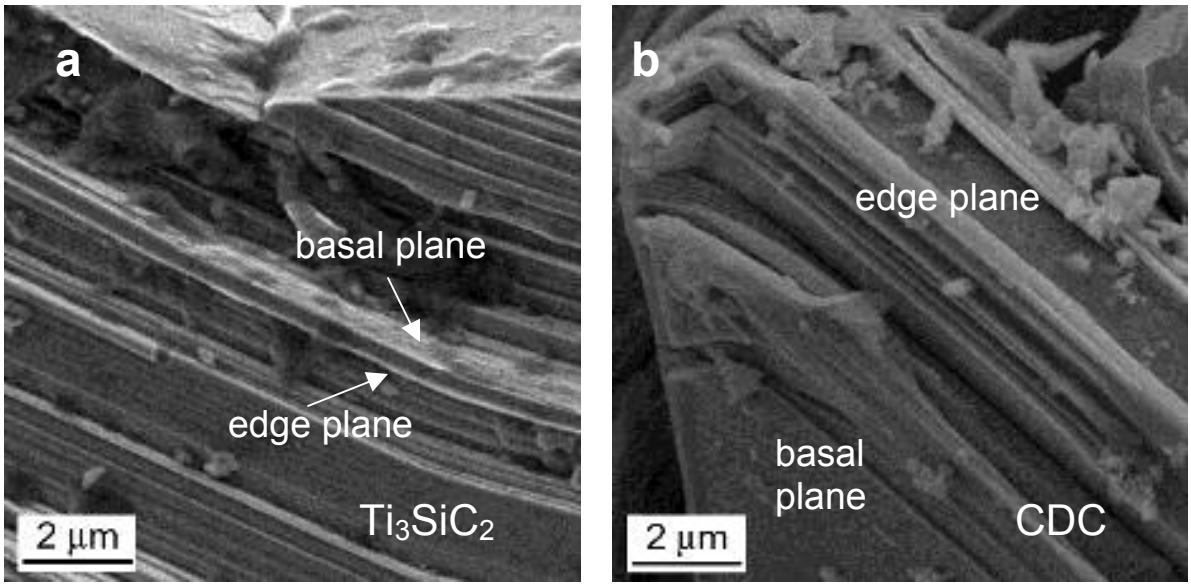

Fig. 4. SEM micrographs of a sample surface **a,** before and **b,** after chlorination at 300ºC. Lamellar structure of Ti_3SiC_2 is clearly seen and it does not change after metal extraction. The sample in (B) is fully amorphous, but maintains the lamellar structure of the carbide. No change in the surface quality or grain morphology occurred after conversion of carbide to carbon.

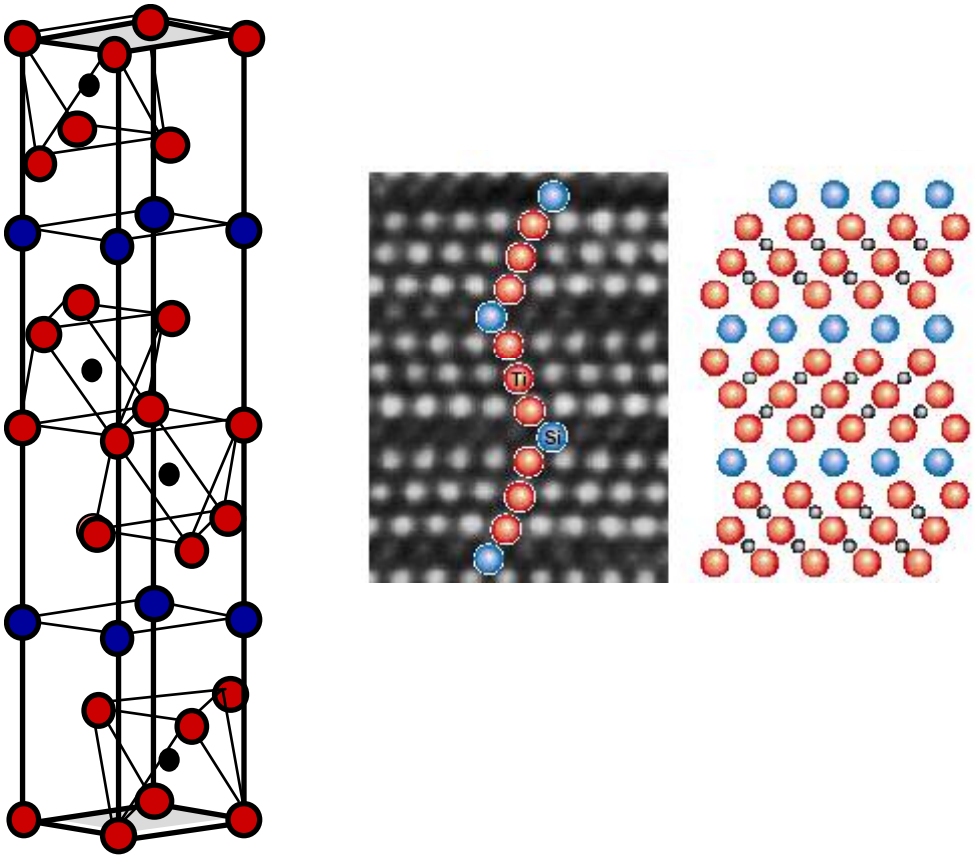

Supplement 1. Unit cell of Ti_3SiC_2, high-resolution TEM image of Ti_3SiC_2 along [110] zone and a schematic of (110) plane. Ti atoms are shown in red, silicon in blue and carbon in black.

Supplement 2. Theoretical density and porosity of carbons produced from different binary carbides and Si_3TiC_2. Porosity range from 53.6% to 83.1% can be covered in CDC. The pore volume can be further increased by oxidative treatment in air or water vapor.

Carbide	Crystal Structure	Density of the carbide, g/cm^3	Theoretical apparent density of CDC, g/cm^3	CDC porosity, %
VC	Cubic	5.48	1.04	53.6
TiC	Cubic	4.92	0.98	56.3
MoC	Hexagonal	8.8	0.98	56.5
WC	Hexagonal	15.8	0.97	57.0
β-SiC	Cubic	3.21	0.96	57.2
TaC	Cubic	14.5	0.90	59.9
NbC	Cubic	7.82	0.89	60.3
Cr_3C_2	Orthorhombic	6.68	0.89	60.4
ZrC	Cubic	6.56	0.76	66.0
CaC_2	Cubic	2.04	0.77	66.0
Al_4C_3	Rhombohedral	2.99	0.75	66.8
SrC_2	Cubic	3.04	0.65	71.0
V_2C	Hexagonal	5.75	0.61	73.1
Ti_3SiC_2	**Hexagonal**	**4.5**	**0.55**	**75.5**
W_2C	Hexagonal	17.3	0.55	75.7
B_4C	Rhombohedral	2.52	0.54	76.0
Mo_2C	Hexagonal	9.12	0.54	76.2
BaC_2	Cubic	3.57	0.53	76.3
Fe_3C	Orthorhombic	7.4	0.49	78.1
Ta_2C	Hexagonal	15	0.48	78.6
Nb_2C	Hexagonal	7.85	0.48	78.9
Cr_4C	Cubic	6.99	0.38	83.1

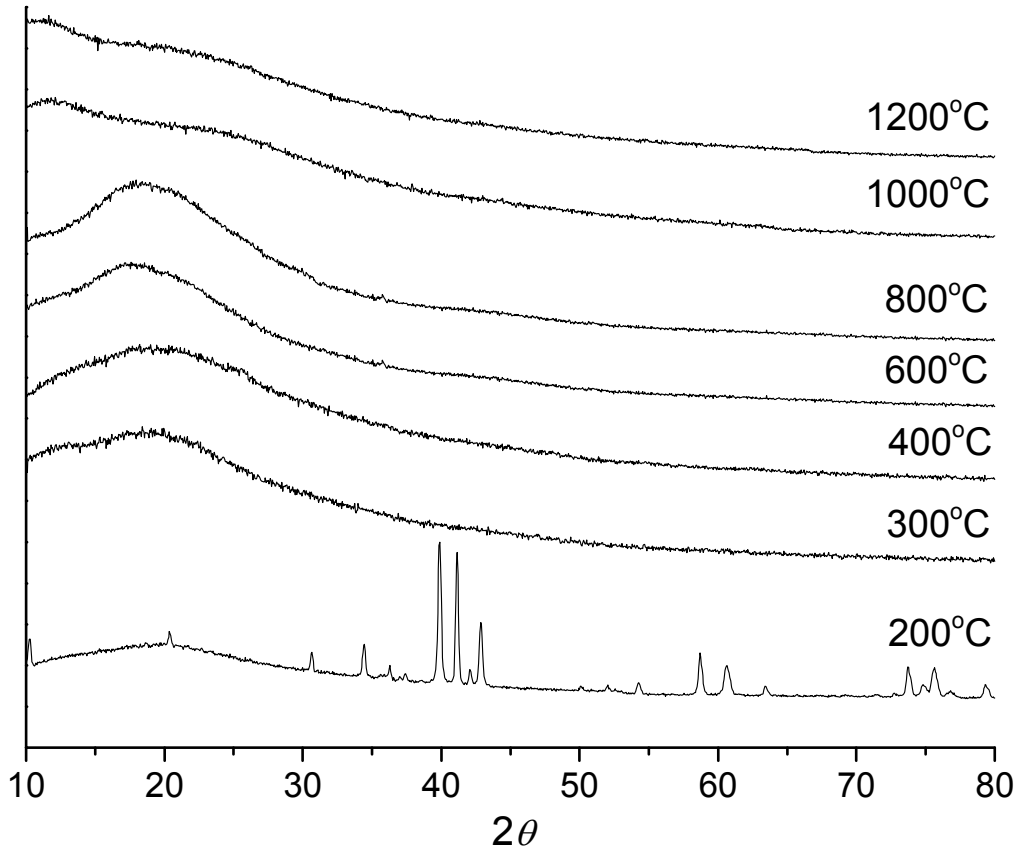

Supplement 3. X-ray diffraction (XRD) spectra of CDC produced at different temperatures (Cu K_α radiation).

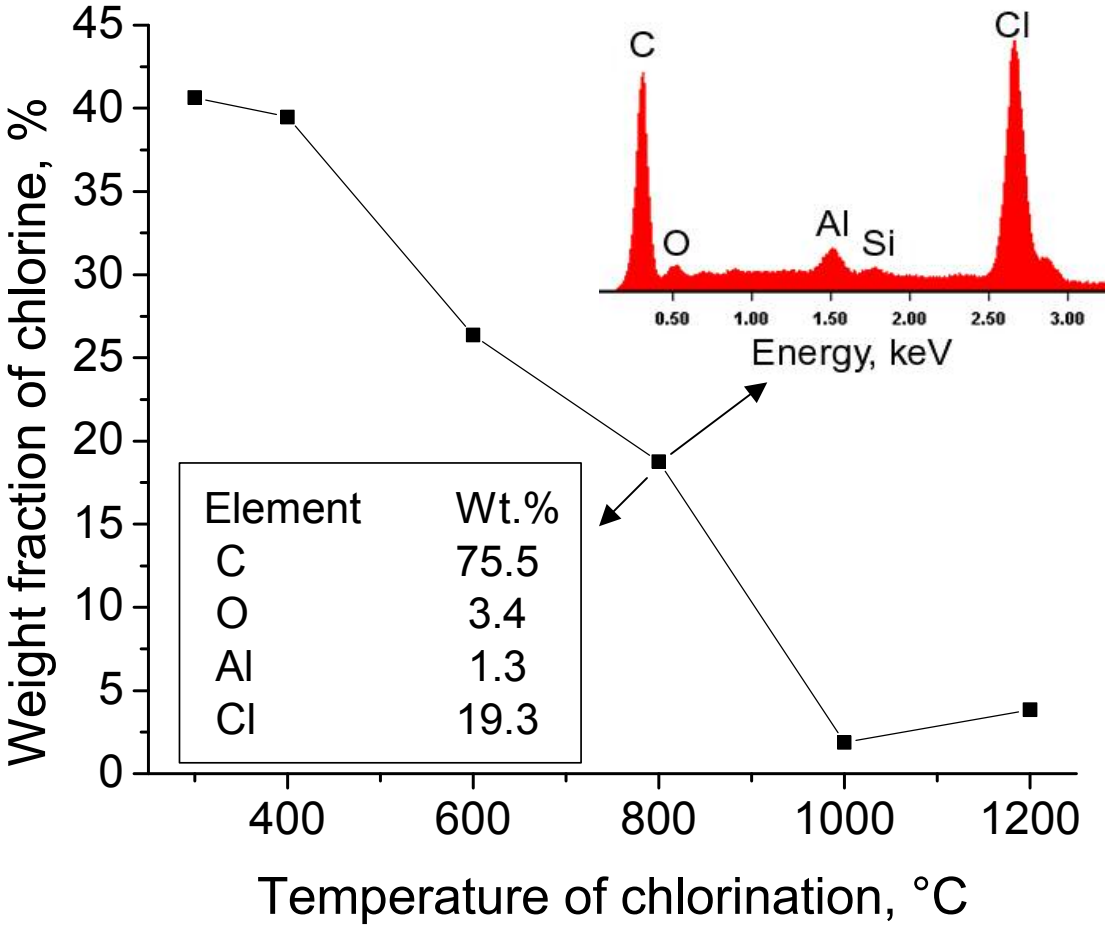

Supplement 4. Weight fraction of chlorine in CDC samples after chlorination based on EDS data (inset). Samples were cooled in Ar. Larger amounts of chlorine can be trapped if cooling is done in chlorine. Efficient chlorine trapping has been achieved for the smallest pore sizes at ambient pressure. Chlorine loaded CDC can be used as a biocide in water/air decontamination and biological protection. Chlorine can be removed from CDC by heating and/or inert gas purging at elevated temperatures [14]. Al signal in the EDS spectrum comes from sample holder. Oxygen comes from water and CO_2 adsorbed from air.